8-3-2018

Role of Stone-Wales Defects on the Interfacial Interactions Among Graphene, Carbon Nanotubes, and Nylon 6: A First-Principles Study

Sanjiv K. Jha
University of Southern Mississippi

Michael Roth
University of Southern Mississippi

Guido Todde
Linnaeus University

J. Paige Buchanan
U.S. Army Corps of Engineers

Robert D. Moser
U.S. Army Corps of Engineers

See next page for additional authors

Role of Stone-Wales defects on the interfacial interactions among graphene, carbon nanotubes, and Nylon 6: A first-principles study

Sanjiv K. Jha,[1,2,3,a)] Michael Roth,[2] Guido Todde,[4] J. Paige Buchanan,[5] Robert D. Moser,[5] Manoj K. Shukla,[3,a)] and Gopinath Subramanian[2]
[1]*Department of Physics, East Central University, Ada, Oklahoma 74820, USA*
[2]*School of Polymer Science and Engineering, The University of Southern Mississippi, Hattiesburg, Mississippi 39406, USA*
[3]*Environmental Laboratory, Engineer Research and Development Center, US Army Corps of Engineers, 3909 Halls Ferry Road, Vicksburg, Mississippi 39180, USA*
[4]*Department of Chemistry and Biomedical Sciences, Linnaeus University, Norra Vägen 49, 392 34 Kalmar, Sweden*
[5]*Concrete and Materials Branch, Engineer Research and Development Center, US Army Corps of Engineers, 3909 Halls Ferry Road, Vicksburg, Mississippi 39180, USA*

(Received 2 April 2018; accepted 12 July 2018; published online 3 August 2018)

We investigate computationally the role of Stone-Wales (SW) defects on the interfacial interactions among graphene, carbon nanotubes (CNTs), and Nylon 6 using density functional theory (DFT) and the empirical force-field. Our first-principles DFT calculations were performed using the Quantum ESPRESSO electronic structure code with the highly accurate van der Waals functional (vdW-DF2). Both pristine and SW-defected carbon nanomaterials were investigated. The computed results show that the presence of SW defects on CNTs weakens the CNT-graphene interactions. Our result that CNT-graphene interaction is much stronger than CNT-CNT interaction indicates that graphene would be able to promote the dispersion of CNTs in the polymer matrix. Our results demonstrate that carbon nanomaterials form stable complexes with Nylon 6 and that the van der Waals interactions, as revealed by the electronic charge density difference maps, play a key stabilizing role on the interfacial interactions among graphene, CNTs, and Nylon 6. Using the density of states calculations, we observed that the bandgaps of graphene and CNTs were not significantly modified due to their interactions with Nylon 6. The Young's moduli of complexes were found to be the averages of the moduli of their individual constituents. *Published by AIP Publishing.* https://doi.org/10.1063/1.5032081

I. INTRODUCTION

Graphene[1] is a two-dimensional single layer carbon sheet where sp^2-hybridized carbon atoms are arranged in a honeycomb structure. It has an extremely high surface area with a theoretical limit of 2630 m^2/g, a tensile strength of 130 GPa and a Young's modulus of 1000 ± 100 GPa,[2] and is one of the strongest materials in existence. Carbon nanotubes (CNTs), on the other hand, are rolled up graphene sheets with a Young's modulus of ~1000 GPa,[3] and are approximately 100 times stronger than stainless steel. The remarkable properties of graphene and CNTs make them promising candidates for a wide range of applications, including chemical sensors, nanoelectronics,[4] and composite materials.[5] However, the low chemical reactivity and insolubility of pristine carbon nanomaterials limit the range of their potential applications and emphasize the need for chemical functionalizations.[6–9]

Complexes made of CNTs and graphene possess several superior properties when compared with the individual carbon nanomaterials, such as enhanced capacitance, stability, and mechanical properties.[10–12] Previous studies have shown that the electrical conductivity of a graphene sheet is enhanced by the addition of CNT,[11,13] and that the π–π intermolecular interactions between CNT and graphene are responsible for the formation of a stable CNT + graphene complex.[11,14,15] Wang *et al.*,[15] computationally investigated the intermolecular interactions between varieties of CNTs (armchair and zigzag conformations) and graphene sheets using density functional theory (DFT) with a generalized gradient approximation (GGA), Perdew-Burke-Ernzerhof (PBE) functional, and Grimme's correction,[16] as implemented in the Vienna *ab initio* simulation package (VASP). The calculations of Wang *et al.*[15] showed that the interaction energies between these carbon nanomaterials mainly depend on the diameters of the nanotubes. However, their computational model did not take into account the influence of stable structural defects on the properties of CNT + graphene complexes. Out of the various known defects in carbon nanomaterials [e.g., vacancies of different size, grain boundaries, Stone-Wales (SW) defects, etc], the Stone-Wales (SW) defects[17] are energetically the most stable ones and have the lowest formation energies (≈5 eV).[18,19] Therefore, we examine the

a)Authors to whom correspondence should be addressed: sjha@ecok.edu and Manoj.K.Shukla@usace.army.mil

influence of SW defects on the properties of CNT + graphene complexes.

The properties of polymers can be significantly modified by the addition of carbon nanomaterials,[5] and the resulting nanocomposites display a significant enhancement in the mechanical,[20–23] thermal,[24] and electrical properties.[25] To achieve the exceptional properties of nanocomposites, it is desirable to optimize the non-covalent interfacial binding of polymer on the surface of carbon nanomaterials.[26] Therefore, understanding the nature and mechanism of interactions between carbon nanomaterials and polymer is essential for the development of desirable polymer nanocomposites.

Nylon 6 is a polymer used in several applications, such as Nylon based nanocomposites, bio-materials, and nanomedicines.[27,28] Previous studies on the interactions between Nylon 6 and carbon nanomaterials[29–34] have indicated a significant enhancement in the mechanical properties of the nanocomposites; however, to the best of our knowledge, the nature and mechanism of interactions between Nylon 6 and carbon nanomaterials have not been yet explored in details. In this paper, we present a comprehensive computational report on the role of SW defects on the interfacial interactions among graphene, CNTs, and Nylon 6. The ability of graphene as a dispersant of CNTs in the polymer matrices and underlying mechanism has also been evaluated.

II. COMPUTATIONAL METHODS

Our computational methods employed both first-principles DFT and empirical force-field levels of theory. Plane-wave DFT calculations were carried out using the Quantum ESPRESSO electronic structure code[35] with the highly accurate van der Waals functional (vdW-DF2).[36,37] The electron-ion interactions were treated with Rappe-Rabe-Kaxiras-Joannopoulos (RRKJ) ultrasoft pseudopotentials[38,39] within GGA-PBE taken from the publicly available repository of the Quantum ESPRESSO distribution. Moreover, the ultrasoft pseudopotentials available for the PBE functional were also used for the vdW-DF2 functional. We are aware of the fact that choosing good pseudopotentials is extremely important part of an electronic-structure calculation. To the best of our knowledge, there has been a common practice in the literature to use the pseudopotentials available for the PBE functional for the vdW-DF2 functional. This approach of combining the vdW-DF2 functional with the pseudopotentials designed for the PBE functional has been successfully employed in several previous studies.[40–43] To validate our computational approach, we first calculated the structures of pristine CNT, graphene, and the CNT + graphene complex and compared them with the available results (described in Sec. III A). Because the dispersive vdW interactions play a key role in the current study, some convergence tests with the semiempirical Grimme's-D2 method[16] (another form of the vdW correction available in Quantum ESPRESSO) were also performed. The electronic states (Kohn-Sham wave functions) were expanded using the plane-wave basis sets with kinetic-energy cutoffs of 30 Ry and 240 Ry for the wave functions and charge densities, respectively. All geometry optimizations were performed using the Broyden-Fletcher-Goldfarb-Shanno (BFGS) algorithm with a force convergence threshold of 10^{-3} Ry/Bohr, and the energies converged to within 10^{-4} Ry in the self-consistent step. The relaxed supercells were used in calculations of electronic charge density difference and electronic density of states (DOS). Because of the relatively large system size (containing up to 259 atoms), only the Γ-point ($k = 0$) of the Brillouin zone was sampled.[43,44] Furthermore, the convergence test with respect to the k-point sampling ($1 \times 1 \times 1$ vs $3 \times 3 \times 1$ k-points tested) confirmed that Γ-point sampling was sufficient to achieve the convergence of computed interaction energy within 0.02 eV/nm. In addition, denser k-point grids were used for the calculations of electronic DOS. The empirical calculations were performed using the class 2 force-field[45] as implemented in the large-scale atomic/molecular massively parallel simulator (LAMMPS) package.[46]

The geometries of the graphene sheet and armchair (8,8) CNT were modeled by periodic orthorhombic supercells with dimensions of $9.88 \times 29.92 \times 46.00$ Å^3 containing 112 and 128 carbon atoms, respectively. These dimensions were identified by the variable-cell geometric optimization (vc-relax) of lattice parameters of graphene. The armchair metallic CNT was specifically chosen in our present study because, according to reported data,[47,48] these CNTs are more reactive than the semiconducting ones and form stronger complexes. The SW defects in carbon nanomaterials were obtained by a local rotation of a C–C bond by 90° about its center, and such a rotation resulted in the transformation of hexagonal rings into pentagonal and heptagonal rings[49] as shown in Figs. 1(b)–1(d).

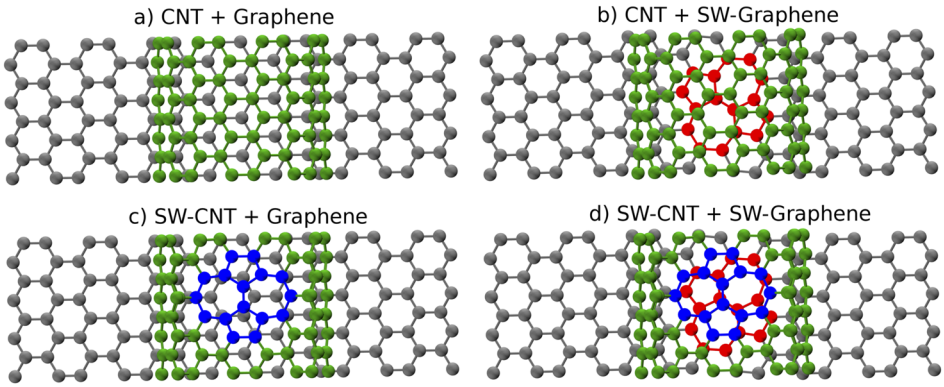

FIG. 1. Optimized geometries of (a) CNT + graphene, (b) CNT + SW-defected graphene, (c) SW-defected CNT + graphene, and (d) SW-defected CNT + SW-defected graphene. The SW-defected sites of graphene are highlighted in red, while those of CNTs are in blue.

Nylon 6 was modeled as a single monomer, with the periodic boundary condition (PBC) along its length. To create a carbon-Nylon 6 composite material, the appropriate supercell has to be selected, where the lattice parameter of Nylon 6 and carbon nanomaterials match along the periodic direction. Comparing the lattice parameter of Nylon 6 ($a = 9.56$ Å)[50] with that of the four unit cells of (8,8) CNT ($a = 9.88$ Å), it is clear that Nylon 6 is slightly shorter than CNT. Therefore to address the length mismatch between the polymer and CNT, the bond lengths of Nylon 6 were a bit stretched. We believe that this is a reasonable assumption to address such length mismatch in periodic calculations (such as ours). To show that such a small "stretch" does not have a significant impact on the computed interaction energies and our assumptions are valid, we further considered a case in which the polymer chain was a bit compressed, and this was attained by considering relatively shorter CNT.

The interactions between CNTs and graphene, Nylon 6 and carbon nanomaterials, and Nylon 6 and CNT + graphene complexes were studied by placing them in orthorhombic supercells with PBC in the graphene plane. To eliminate the effects of artificial periodicity on the studied systems, we maintained a sufficiently large vacuum spacing in the direction orthogonal to the graphene plane (z-axis). Prior to the geometry optimizations of the complexes, the geometries of individual CNTs, graphene, and Nylon 6 were optimized. While combining the CNT with graphene, the center of the benzene ring of CNT was positioned directly over a carbon atom of the graphene [see Fig. 1(a)] because of the higher stability (stronger interaction) of such configurations.[51,52] The interactions between CNTs and graphene sheets were examined in four specific cases: (a) CNT + graphene, (b) CNT + SW-defected graphene, (c) SW-defected CNT + graphene, and (d) SW-defected CNT + SW-defected graphene, as shown in Fig. 1.

A. Interaction energy calculation

The interaction energy, E_{int}, between two species A and B was computed as

$$E_{\text{int}}(AB) = E_{\text{AB}} - E_{\text{A/AB}} - E_{\text{B/AB}}, \tag{1}$$

where AB represents the complex, E_{AB} is the total energy of the complex, $E_{\text{A/AB}}$ is the total energy of the species A within the geometry of the complex, and $E_{\text{B/AB}}$ is the total energy of the species B within the geometry of the complex. With this definition, negative values of interaction energies correspond to the stable configurations. All the computed interaction energies were normalized by the length of the CNT (the cell dimension along the x-direction).[15,43]

B. Charge density difference calculation

To understand the nature of interaction in the complex formation of two species A and B, the electronic charge density difference maps were examined. For the fully relaxed, minimum total-energy configuration, the charge density difference was calculated as

$$\Delta\rho = \rho_{\text{AB}} - \rho_{\text{A/AB}} - \rho_{\text{B/AB}}, \tag{2}$$

where ρ_{AB}, $\rho_{\text{A/AB}}$, and $\rho_{\text{B/AB}}$ are the electronic charge densities of the complex, species A, and species B, respectively. In the calculations of the latter two quantities, the atomic positions were kept fixed at precisely the same positions as they were in the AB system. The charge density difference maps were generated using the visualization for electronic and structural analysis (VESTA) package.[53]

C. Young's modulus calculation

Young's modulus was calculated using the second derivative of total energy with respect to strain as

$$Y = \frac{1}{V_0}\frac{\partial^2 E}{\partial \varepsilon^2}, \tag{3}$$

where V_0 is the equilibrium volume (volume of the unstrained system), E is the total energy, and ε is the engineering strain. The volume of the graphene sheet was obtained using $V_0 = abt$, where a, b, and t represent length, width, and thickness, respectively. Similarly, the volume of CNT was obtained using $V_0 = 2\pi r l_0 t$, where r, l_0, and t represent radius, equilibrium (relaxed) length, and thickness, respectively. In our calculation, the radius, r, of the CNT was evaluated to be 5.49 Å ($= \frac{10.98}{2}$ Å). To avoid the confusion on the definition of the thickness, all previous studies on graphene and CNT have considered the interlayer separation of graphite as a thickness for graphene and CNT.[43,54,55] In all our calculations, we therefore used $t = 3.33$ Å, the equilibrium separation between graphene and CNT, as a thickness for both graphene and CNT. To obtain the Young's modulus, we performed a series of total energy calculations for unstrained and strained structures. The energies of unstrained structures were obtained by the variable-cell relaxations. The energies of strained structures were obtained by applying a small strain in the interval, $\varepsilon \in [-0.02, 0.02]$, and re-scaling the new coordinates of the atoms to fit within the new cell dimensions. After each increment of the strain, only atomic positions of the systems were reoptimized keeping the cell dimensions fixed. The values of curvature (i.e., $\frac{\partial^2 E}{\partial \varepsilon^2}$) at the energy minima ($\varepsilon = 0$) were obtained using the second-order polynomial fitting of the energy-strain data.

III. RESULTS AND DISCUSSION

A. Interactions between carbon nanotubes and graphene

In order to validate our computational approach, we first calculated the structures of pristine CNT, graphene, and the CNT + graphene complex, and compared them with the available results. For pristine graphene, our plane-wave DFT calculations predicted an equilibrium C–C bond length of 1.42 Å, which was in good agreement with previous reports.[56,57] Our calculations showed the equilibrium interlayer spacing between CNT and graphene to be 3.33 Å, which was consistent with the experimentally measured value of 3.34 Å.[58] At this separation, the CNT-graphene interactions are governed by long range van der Waals forces.

Optimized geometries for various CNT + graphene complexes are shown in Fig. 1, where four different possible combinations of CNTs and graphene are considered. The

TABLE I. Computed interaction energies between CNTs and graphene.[a]

Configuration	E_{int} (eV/nm) DFT	Force-field
(a) CNT + graphene	−1.61	−1.67
(b) CNT + SW-graphene	−1.64	−1.68
(c) SW-CNT + graphene	−1.52	−1.38
(d) SW-CNT + SW-graphene	−1.50	−1.38

[a]Results were obtained using the vdW-DF2 functional and class 2 force-field.

computed interaction energies (per unit length of CNT) between CNTs and graphene sheets in these configurations are summarized in Table I, which includes the values obtained from both DFT and empirical force-field levels of theory. All the computed interaction energies are negative, indicating that all CNT + graphene complexes are thermodynamically stable and their formations are energetically favorable. For the complex of pristine CNT and pristine graphene [see Fig. 1(a)], our DFT calculations with vdW-DF2 functional predicted the interaction energy to be −1.61 eV/nm with almost no deformation present in the geometries of CNT and graphene due to the complex formation. Because the dispersive vdW forces play an important role in our current study, some test calculations with the semiempirical Grimme's-D2 method[16] were also performed. The Grimme's method yielded the interaction energy between CNT and graphene to be −1.57 eV/nm, which agreed exceptionally well with the vdW-DF2 result. Furthermore, the empirical force-field calculations resulted in the interaction energy of −1.67 eV/nm, which is in excellent agreement with our DFT results. The consistency of the interaction energies computed using vdW-DF2, Grimme's-D2, and empirical force-field methods confirms the validity of our computational approach.

Wang *et al.*[15] reported the interaction energy between (8,8) CNT and graphene to be ∼−3.50 eV/nm, which was approximately double of that obtained in our current study. We reiterate that the calculations of Wang *et al.*[15] were performed with the GGA-PBE functional and Grimme's correction as implemented in the VASP package. Their calculations further yielded the interaction energies of graphene sheets with (10,10) and (6,6) CNTs to be ∼−3.80 eV/nm and −3.03 eV/nm, respectively. To probe the origins of the mismatch between our study and that predicted by Wang *et al.*,[15] we examined the interactions of graphene sheets with CNTs of three different diameters [(6,6), (8,8), (10,10)] using vdW-DF2 and Grimme's-D2 methods. A detailed comparison of the computed interaction energies between our study and those predicted by Wang *et al.*[15] is provided in Table II. Our calculations showed the interaction energy between (10,10) CNT and graphene (using the exact same conditions as used by Wang *et al.*,[15] such as, the cell dimension 2.48 × 43.02 × 50.00 Å^3, *k*-points 11 × 1 × 1, and the exchange-correlation functional GGA-PBE with Grimme's correction) to be −1.81 eV/nm. Similarly, the interaction energy between (6,6) CNT and graphene was computed to be −1.41 eV/nm. Our results presented in Table II show that the interaction energies between CNTs and graphene computed using vdW-DF2 and Grimme's-D2 methods agree to within 0.00-0.04 eV/nm. These observations clearly suggest that the values of interaction energies obtained in our study are approximately half of those obtained by Wang *et al.*[15] To further examine if the dispersive vdW interactions were properly treated in our calculations, we recomputed these interaction energies using the GGA-PBE functional (without a dispersion correction), which all yielded the interaction energy of zero (nearly), as shown in Table II. This result was expected because the GGA functional has been well-known to underestimate the interaction energy, as it neglects the long-range dispersive vdW interactions.[41,59–61] This corroborates with the fact that weak dispersive vdW interactions are responsible for CNT-graphene interactions, which are not accounted in the GGA approximation. This result further confirmed that the dispersive vdW interactions have been properly taken into account in our calculations via vdW-DF2 and Grimme's-D2 approaches.

We attempted all potential routes to probe the origins of such a mismatch by reproducing the interaction energies reported in Ref. 15 using the exact same conditions (GGA-PBE and Grimme's method for the long-range van der Waals interaction, the same *k*-points, etc). All of our results consistently suggested that the values of interaction energies obtained in our study were approximately half of those obtained in the study of Wang *et al.*[15] Despite our computed results followed the trend predicted by Wang *et al.*,[15] the interaction energies increase with the increasing diameter of the nanotubes; however, we believe that the absolute values of interaction energies obtained by Wang *et al.*[15] are consistently overestimated compared to our results.

The presence of SW defects in the CNT pushed the rings belonging to the defected carbon atoms into the tube [inwards, see Fig. 2(c)], resulting in deformation. This resulted in an increase in the CNT-graphene separation from 3.33 Å up to ∼4.05 Å (in the vicinity of defected rings), thereby decreasing the interfacial interaction energies. We did not observe any significant deformations in the geometries of graphene or

TABLE II. Detailed comparison of computed interaction energies (eV/nm) between our study and the results of Wang *et al.*[15]

System	This work vdW-DF2	Grimme's-D2	GGA-PBE	Wang *et al.*[15] Grimme
(6, 6) CNT + graphene	−1.41	−1.42	+0.01	−3.03
(8,8) CNT + graphene	−1.61	−1.57	−0.08	∼−3.50
(10, 10) CNT + graphene	−1.81	−1.81	−0.04	∼−3.80

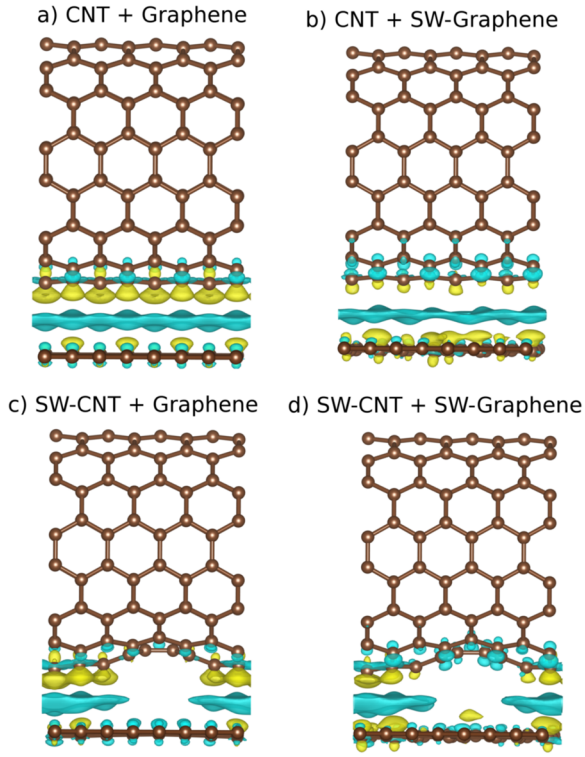

FIG. 2. Isosurfaces depicting electronic charge density difference for (a) CNT + graphene, (b) CNT + SW-defected graphene, (c) SW-defected CNT + graphene, and (d) SW-defected CNT + SW-defected graphene as obtained from the vdW-DF2 functional. Yellow and cyan regions represent isosurfaces for gain and loss of charge densities, respectively. The isosurface corresponds to 1.7×10^{-4} |e|/Bohr^3.

CNTs due to the complex formations. Furthermore, the interaction energies obtained using the force-field method showed good agreement with the values obtained from the electronic structure method (converged to within ∼0.14 eV/nm) and indicated that the class 2 force-field is suitable to study the properties of carbon-based materials.

We further tested our model by computing the interaction energy between two infinitely long CNTs. Our DFT calculations predicted the interaction energy to be −1.08 eV/nm, which indicated that CNT interacts much strongly with graphene than with another CNT (by 0.53 eV/nm). Considering another van der Waals-DFT approach, we would like to mention that Kleis *et al.*[62] calculated the interaction energy between two (8,0) CNTs to be ∼−0.75 eV/nm, which is comparable to the interaction energy of −1.08 eV/nm that we have calculated for (8,8) CNTs. The observed difference in computed interaction energies between our calculation and those obtained in Ref. 62 (−1.08 eV/nm vs ∼−0.75 eV/nm) is attributed to the difference in the diameters of CNTs employed in these studies [(8,8) vs (8,0)]. In the absence of graphene, the interaction between two long CNTs in the sample is large (strong) enough to agglomerate due to van der Waals forces. Our result that CNT-graphene interaction is much stronger than CNT-CNT interaction, predicts that graphene should be able to promote the dispersion of CNTs in the polymer matrix, resulting in an enhancement in mechanical properties of nanocomposites containing CNT-graphene nanocarbons.

The electronic charge density difference maps for the interactions between CNTs and graphene are shown in Fig. 2, which demonstrate how the charge density changes during the interaction process. In these plots, the charge accumulation and charge depletion regions are represented by yellow and cyan colors, respectively. In all of the four cases shown, no charge accumulation could be seen between the CNTs and graphene. The existence of cyan regions between CNTs and graphene indicate that the charge rearrangements are not accompanied by electron density enhancement in the middle region. All of the electronic density difference maps shown in Fig. 2 follow the same pattern and revealed that there is no covalent character in these interactions, and the systems are stabilized via dispersion forces. In the covalent interaction, there is accumulation of charge density at the center of the bond, while there is depletion of charges at the corresponding bonding centers.[60,63] The reverse is revealed in the present case. Moreover, the reduction of electronic charge density at the center of the interacting region observed in our study is similar to the one obtained by Rohrer and Hyldgaard for the vdW-bonded graphane bilayers.[64] The maps shown in Figs. 2(c) and 2(d) clearly indicate that the interactions of SW-defected CNTs with graphene are weaker. This observation is also supported by the data presented in Table I, where the presence of SW defects in CNT has shown to lower the interaction energies between CNT and graphene. Our observation suggests that the CNT-graphene interaction is weak, and mostly due to the dispersion force. We reiterate that the concentrations of SW defects in our study were low, i.e., 1 defect per 128 atoms of CNT (or 1 defect per 112 atoms of graphene); a higher concentration of such defects could have a more significant impact on the interfacial interactions.

We also analyzed the electronic DOS. The calculated DOS for four different CNT + graphene complexes are shown in Fig. 3, where the DOS of the individual CNT and graphene are also included for the reference. The zero energy in Fig. 3 is set at the Fermi level. For the SW-defected graphene, the computed DOS showed clear signatures of additional impurity bands near the Fermi level. The DOS of CNT + graphene complexes are nearly a sum of the DOS values of their individual constituents. On comparing the DOS between the complexes and the individual CNT, we do not observe any significant shift in the van Hove singularities[65] of the CNTs, which is consistent with the results of Wang *et al.*[15]

In order to investigate the effect of interactions on the mechanical properties of carbon nanomaterials, the Young's moduli were computed. For comparison, we first computed the moduli of individual graphene and CNTs. The variations of total energies of carbon nanomaterials as a function of strains are shown in Fig. 4. The negative and positive values of strain correspond to "compression" and "elongation" of carbon nanomaterials, respectively. Using the second order polynomial fitting of energy-strain data, the values of curvature E'' $(= \frac{\partial^2 E}{\partial \varepsilon^2})$ were obtained. The computed Young's moduli of carbon nanomaterials are summarized in Table III. For pristine graphene and CNT, we obtained the values of Young's moduli to be 1068 GPa and 1032 GPa, respectively, which are in good agreement with the experimental values of 1000 ± 100 GPa for graphene[2] and ∼1000 GPa for the

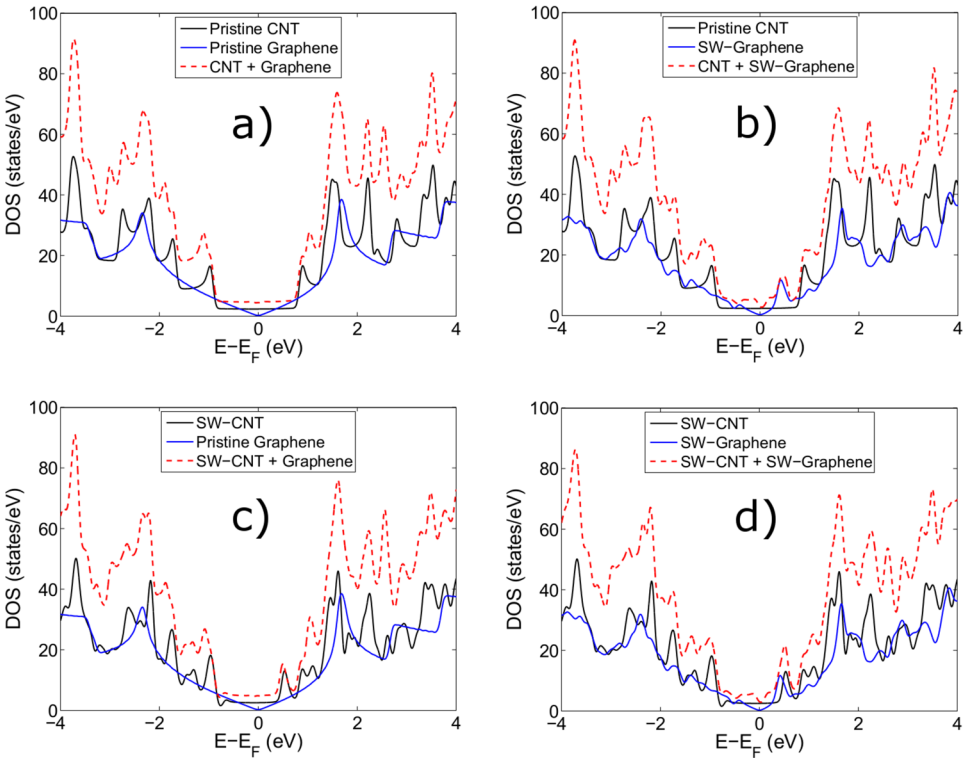

FIG. 3. Calculated electronic densities of states (DOS) of (8,8) CNT (in black color), graphene (in blue), and the CNT + graphene complex (in dotted red) for the interactions of (a) CNT + graphene, (b) CNT + SW-defected graphene, (c) SW-defected CNT + graphene, and (d) SW-defected CNT + SW-defected graphene. The zero energy corresponds to the Fermi level.

CNT.[3] We also observed that the presence of SW defects in carbon nanomaterials lowers their Young's moduli, and this behavior is in qualitative agreement with the results of Hao *et al.*,[66] where the Young's modulus of graphene was found to decrease with the increasing concentration of SW defects.

To investigate the influence of interactions between CNT and graphene on their mechanical properties, we next computed the Young's moduli of various CNT + graphene complexes. The variations of total energies of CNT + graphene complexes as a function of strains are shown in Fig. 5, and the computed Young's moduli are summarized in Table IV. Our computed result showed the modulus of the pristine CNT + pristine graphene complex to be 1048 GPa. When comparing the Young's moduli of various CNT + graphene complexes with their constituents (see Table III), we find that the moduli of complexes are the averages of the moduli of their individual constituents.

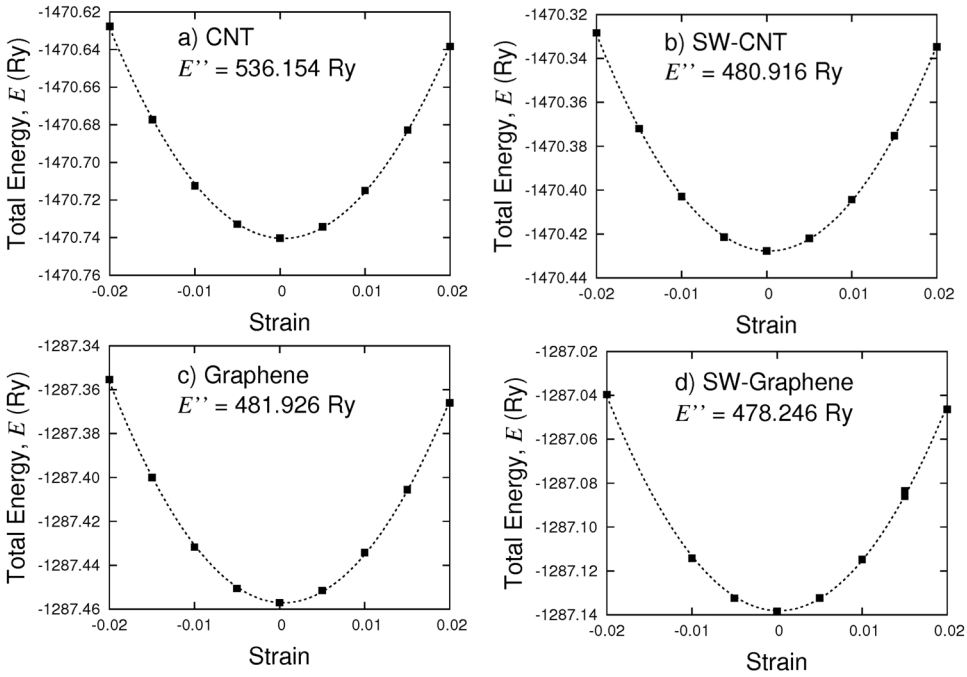

FIG. 4. Variation of total energy as a function of strain for (a) pristine CNT, (b) SW-defected CNT, (c) pristine graphene, and (d) SW-defected graphene. The dotted lines represent the quadratic polynomial fits, and E'' is the curvature of energy-strain data.

TABLE III. Simulated Young's moduli of individual carbon nanomaterials.

	Y (GPa)	
Configuration	This work	Experiment
(a) Pristine graphene	1068	1000 ± 100 (Lee *et al.*)[2]
(b) SW-graphene	1056	...
(c) Pristine CNT	1032	~1000 (Lau *et al.*)[3]
(d) SW-CNT	919	...

TABLE IV. Simulated Young's moduli of CNT + graphene complexes.

Configuration	*Y* (GPa)
(a) CNT + graphene	1048
(b) CNT + SW-graphene	1046
(c) SW-CNT + graphene	982
(d) SW-CNT + SW-graphene	974

B. Interactions between Nylon 6 and carbon nanomaterials

After studying the interfacial interactions between CNTs and graphene, we extend our model to investigate the interaction of Nylon 6 with these carbon nanomaterials. We study the simplest model by considering the interactions (adsorption) of a monomer of Nylon 6 with carbon nanomaterials. In the literature, a similar model was used by Jilili *et al.* to study the non-covalent functionalization of CNTs and graphene by a conjugated polymer.[67] As mentioned in Sec. II, the Nylon 6 was slightly stretched (or compressed) due to the length mismatch between the polymer and the CNT/graphene, which induces a little bit of tension (or slack) in the polymer.

Optimized geometries for the complexes of Nylon 6 and carbon nanomaterials are shown in Fig. 6, where both the stretched [panels (a) and (b)] and the compressed [panels (c) and (d)] forms of Nylon 6 are considered. The computed interaction energies between Nylon 6 and carbon nanomaterials are summarized in Table V. For the interaction of the stretched monomer of Nylon 6 with pristine CNT [see Fig. 6(a)], the interaction energy at the DFT level of theory was computed to be −0.42 eV/nm, and the shortest equilibrium distance between the CNT and the non-hydrogen atoms of Nylon 6 was found to be ~3.4 Å. This indicates that the interaction is mediated by long-range van der Waals forces. The results presented in Table V also suggest that Nylon 6 interacts much more strongly with the flat surface of graphene than with the curved surface of CNT due to the larger surface area of graphene. This result is qualitatively consistent with the previous studies of Jilili *et al.*,[67] for the interaction of CNT/graphene with a conjugated polymer, and Rajesh *et al.*,[56] for the interaction of CNT/graphene with amino acids, where similar findings have been reported. On the other hand, the interaction energies of the compressed monomer of Nylon 6 with CNT and with graphene were computed to be −0.50 eV/nm and −0.66 eV/nm, respectively. Thus, the monomer chain interacts only weakly with CNT and graphene, as the interaction energies obtained for stretched and compressed forms of Nylon 6 are low and within 0.14 eV/nm of each other. The presence of SW defects in carbon nanomaterials did not make any significant effect on the computed interaction energies. This observation is qualitatively consistent with the previous computational result (DFT) of Hassan *et al.*,[61] which predicted that the dispersion binding of a benzene on defected graphene is similar to the pristine one. Furthermore, we observed that the results obtained from the force-field method followed the trend predicted by the electronic structure method, and these two results agreed to within 0.11 eV/nm.

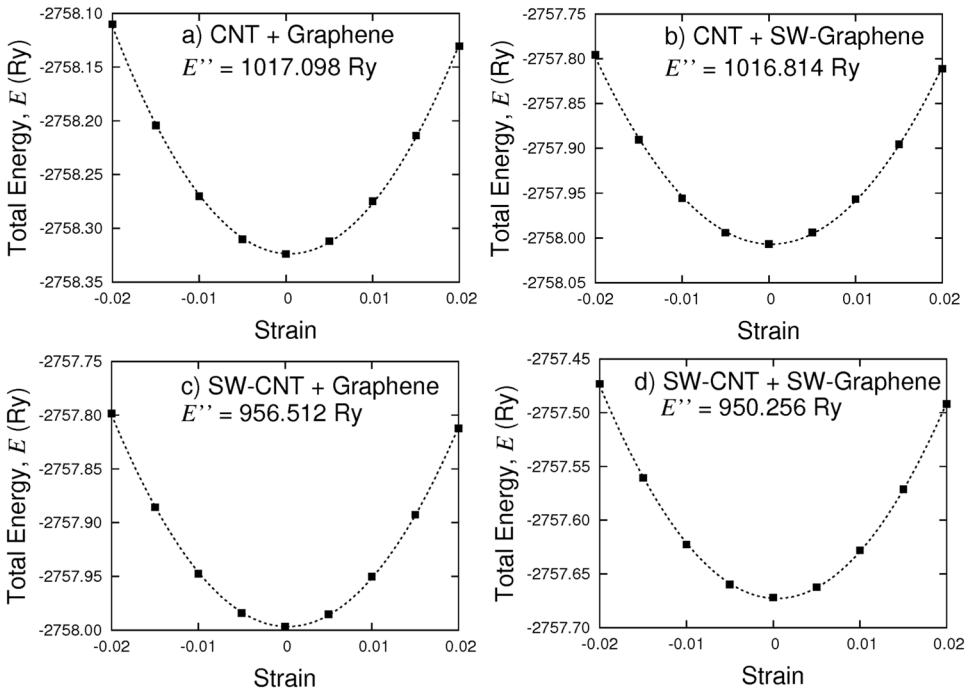

FIG. 5. Variation of total energy as a function of strain for (a) CNT + graphene, (b) CNT + SW-defected graphene, (c) SW-defected CNT + graphene, and (d) SW-defected CNT + SW-defected graphene. The dotted lines represent the quadratic polynomial fits, and E'' is the curvature of energy-strain data.

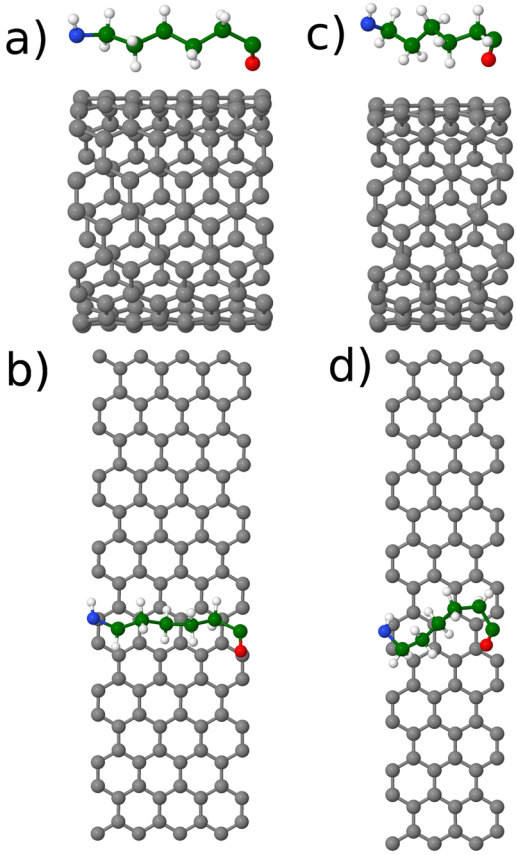

FIG. 6. Optimized geometries for the interactions of Nylon 6 with carbon nanomaterials, where both the stretched [panels (a) and (b)], and the compressed [panels (c) and (d)] forms of Nylon 6 are considered. Atom color scheme: C atoms of graphene/CNT and Nylon 6 are represented in gray and green, respectively; O in red, N in blue, and H in white.

The electronic charge density difference maps for the interactions of a stretched monomer of Nylon 6 with carbon nanomaterials are shown in Fig. 7. These maps indicate a net loss of electronic charge in regions between CNTs (or graphene) and Nylon 6, which is thought to be characteristics of van der Waals interactions. We also note that these plots are similar to those obtained for the CNT-graphene interactions in the previous Sec. III A. We also computed electronic charge density difference maps of the complex involving the compressed monomer of Nylon 6 with carbon nanomaterials, which were found to be similar to those shown in Fig. 7 (see Fig. S1 of the supplementary material).

TABLE V. Computed interaction energies between Nylon 6 and carbon nanomaterials.[a]

	E_{int} (eV/nm)			
	Stretched Nylon 6		Compressed Nylon 6	
Configuration	DFT	Force-field	DFT	Force-field
CNT + Nylon 6	−0.42	−0.35	−0.50	−0.41
SW-CNT + Nylon 6	−0.42	−0.34	...	...
Graphene + Nylon 6	−0.52	−0.44	−0.66	−0.55
SW-graphene + Nylon 6	−0.53	−0.45	...	...

[a]Results were obtained using the vdW-DF2 functional and class 2 force-field.

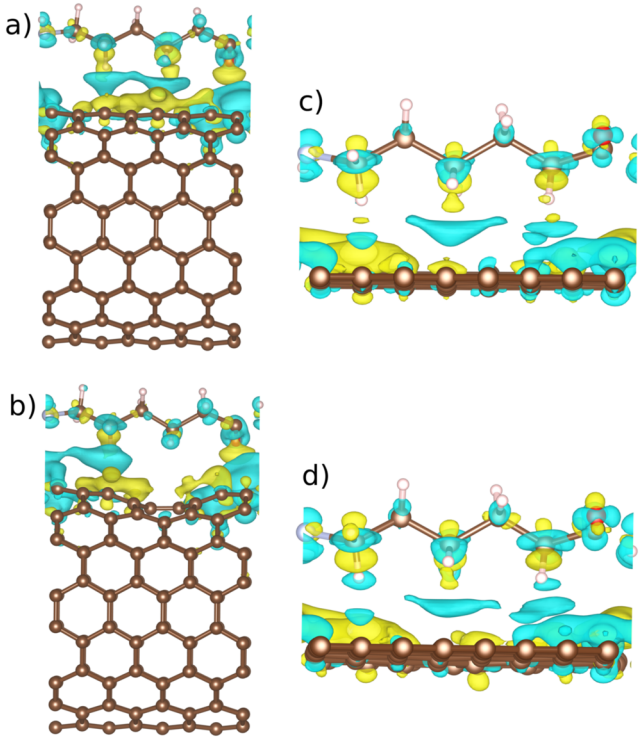

FIG. 7. Isosurfaces depicting electronic charge density difference for the interactions of Nylon 6 (stretched) with (a) pristine CNT, (b) SW-defected CNT, (c) pristine graphene, and (d) SW-defected graphene as obtained from the vdW-DF2 functional. Yellow and cyan regions represent isosurfaces for gain and loss of charge densities, respectively. The isosurface corresponds to 1.7×10^{-4} |e|/Bohr^3.

The electronic DOS for the interactions of a stretched monomer of Nylon 6 with carbon nanomaterials are shown in Fig. 8, where the DOS of individual CNT, graphene, and Nylon 6 are also included for comparison. The computed DOS indicates that Nylon 6 has the highest occupied molecular orbital-lowest unoccupied molecular orbital (HOMO-LUMO) energy gap of ~4.4 eV. The DOS of complexes exhibit additional peaks, indicating the interactions between the orbitals of Nylon 6 and carbon nanomaterials. Analyzing the DOS of complexes and their constituents, we observed that the DOS of carbon nanomaterials are not significantly affected due to their interactions with Nylon 6. We also computed the DOS of the complex involving the compressed monomer of Nylon 6 with carbon nanomaterials, which are shown in Fig. S2 of the supplementary material. Our results suggest that the interactions between Nylon 6 and carbon nanomaterials are weak, and therefore, we do not observe significant modifications in the bandgaps of carbon nanomaterials. Our computed results demonstrated that the stability and electronic properties of complexes are not significantly affected due to a small "stretch/compress" of Nylon 6; therefore all further calculations will employ only the stretched model of Nylon 6 for the convenience.

The Young's moduli of complexes of Nylon 6 and carbon nanomaterials were obtained using the energy-strain curve shown in Fig. 9. The computed elastic moduli of the complexes are summarized in Table VI. For comparison, the computed Young's moduli of individual CNTs (or graphene) are also included in parentheses. We find that the Young's modulus of

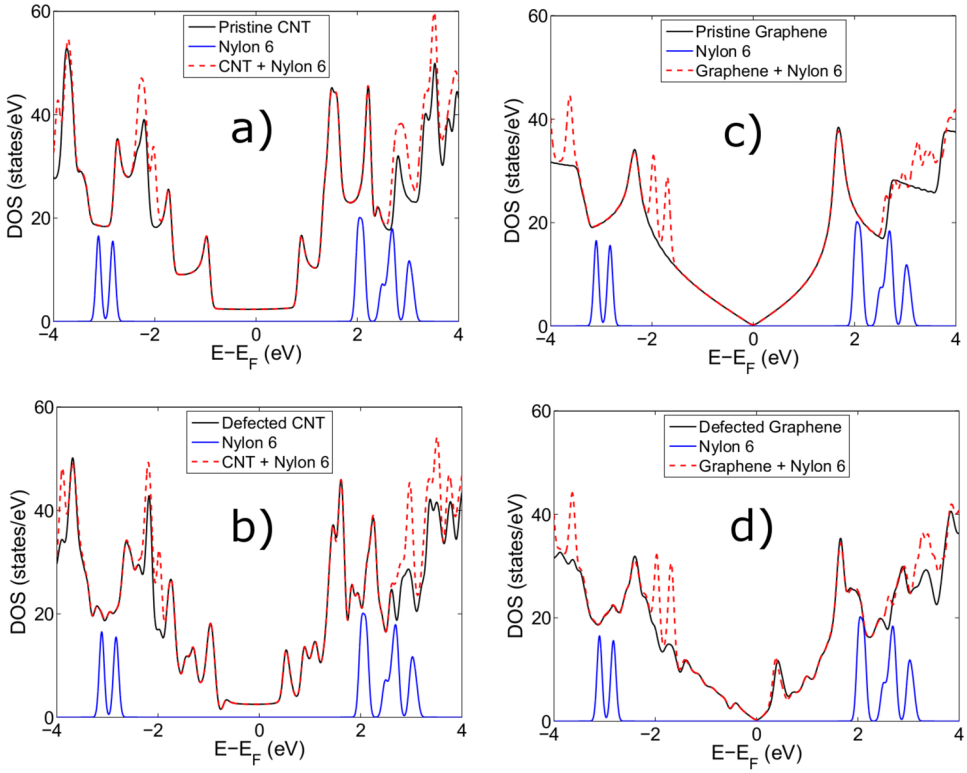

FIG. 8. DOS for the interactions of Nylon 6 (stretched) with (a) pristine CNT, (b) SW-defected CNT, (c) pristine graphene, and (d) SW-defected graphene. The DOS of CNT (or graphene) is shown in black color, Nylon 6 in blue, and the complex in dotted red. The zero energy corresponds to the Fermi level.

pristine CNT is decreased from 1032 GPa to 1016 GPa, while that of the graphene is decreased from 1068 GPa to 1048 GPa because of their interactions with Nylon 6. Similar results were obtained for the complexes of Nylon 6 and SW-defected carbon nanomaterials. We also note that the presence of SW defects in carbon nanomaterials diminished their Young's moduli. Overall, the interactions of Nylon 6 decreased the Young's moduli of carbon nanomaterials in a range of ∼1.5%–3.0%. We reiterate that these Young's moduli were calculated for the interactions of a single polymer chain of Nylon 6 with CNT/graphene.

C. Interactions between Nylon 6 and CNT + graphene complexes

Since the CNT was found to interact much strongly with graphene than with another CNT, we further examined the interactions of Nylon 6 with CNT + graphene complexes using

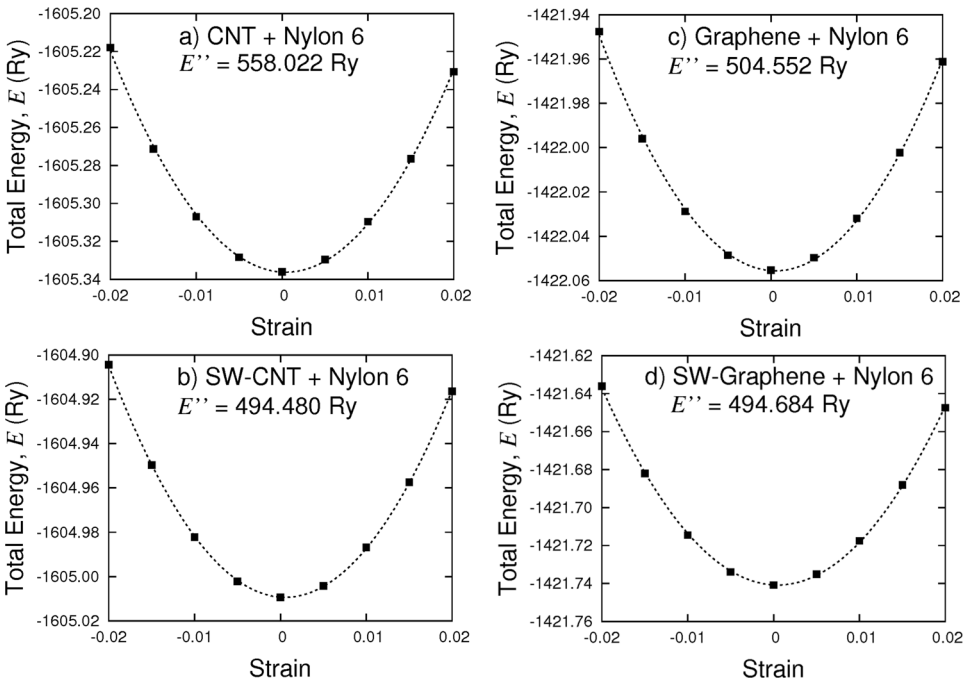

FIG. 9. Variation of total energy as a function of strain for the interactions of Nylon 6 (stretched) with (a) pristine CNT, (b) SW-defected CNT, (c) pristine graphene, and (d) SW-defected graphene. The dotted lines represent the quadratic polynomial fits, and E'' is the curvature of energy-strain data.

TABLE VI. Simulated Young's moduli of complexes of Nylon 6 and carbon nanomaterials. The values in parentheses indicate moduli of individual carbon nanomaterials (without Nylon 6).

Configuration	Y (GPa)
(a) CNT + Nylon 6	1016 (1032)
(b) SW-CNT + Nylon 6	895 (919)
(c) Graphene + Nylon 6	1048 (1068)
(d) SW-graphene + Nylon 6	1025 (1056)

the vdW-DF2 functional. For each of four CNT + graphene complex represented in Fig. 1, two adsorption positions of Nylon 6 were studied, a totaling of eight. Therefore, the interaction energies between Nylon 6 and CNT + graphene complexes were computed for eight different configurations, where both pristine and SW-defected carbon nanomaterials were considered. For such a system, the interaction energy was evaluated using the formula

$$E_{\text{int}}(ABC) = E_{\text{ABC}} - E_{\text{A/ABC}} - E_{\text{BC/ABC}}, \quad (4)$$

where ABC represents the complex of Nylon 6 and CNT + graphene, E_{ABC} is the total energy of the complex, $E_{\text{A/ABC}}$ is the total energy of Nylon 6 within the geometry of the complex, and $E_{\text{BC/ABC}}$ is the total energy of CNT + graphene within the geometry of the complex.

Optimized geometries of the complexes of Nylon 6 and CNT + graphene are shown in Fig. 10 (only two configurations shown for the convenience). As clearly seen, the only difference between the geometries of these two complexes is the position of Nylon 6 relative to CNT + graphene complex. In the first case (Fig. 10, left), Nylon 6 is adsorbed closer to the CNT surface, while on the second one (Fig. 10, right), it is adsorbed closer to the graphene surface. The computed

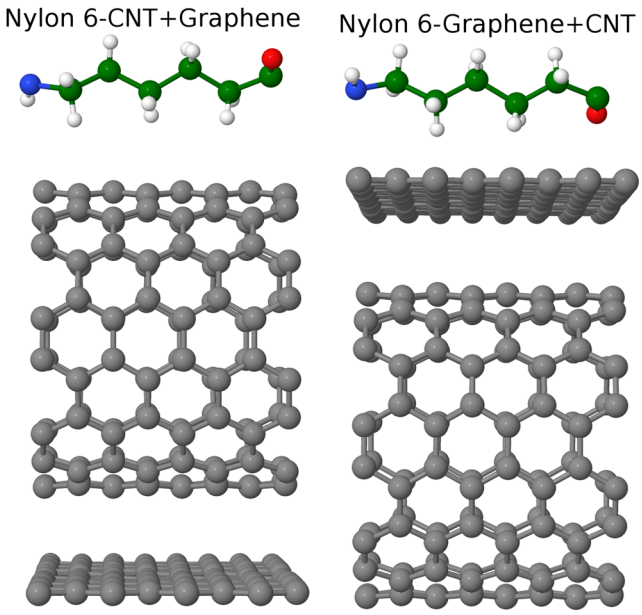

FIG. 10. Optimized geometries for the interactions of Nylon 6 with the CNT + graphene complex. For each of four CNT + graphene complex represented in Fig. 1, two adsorption positions of Nylon 6 are plausible, a totaling of eight.

TABLE VII. Computed interaction energies between Nylon 6 and CNT + graphene complexes as obtained from the vdW-DF2 functional.

Configuration	E_{int} (eV/nm)
Nylon 6-CNT + graphene	−0.41
Nylon 6-graphene + CNT	−0.57
Nylon 6-CNT + graphene (SW)	−0.40
Nylon 6-graphene (SW) + CNT	−0.56
Nylon 6-CNT (SW) + graphene	−0.41
Nylon 6-graphene + CNT (SW)	−0.56
Nylon 6-CNT (SW) + graphene (SW)	−0.40
Nylon 6-graphene (SW) + CNT (SW)	−0.56

interaction energies between Nylon 6 and CNT + graphene in eight different configurations are summarized in Table VII, which clearly demonstrates that Nylon 6 forms stable complexes with CNT + graphene. We find that the interaction energy of Nylon 6 with CNT + graphene is −0.41 eV/nm when the Nylon 6 is adsorbed closer to the CNT surface (Fig. 10, left). The strength of the interaction was increased to −0.57 eV/nm when Nylon 6 was adsorbed closer to the flat graphene surface (Fig. 10, right). Analyzing the data of Table VII, we find that the strength of interaction between Nylon 6 and CNT + graphene is always higher (more stable) for the adsorption of Nylon 6 closer to the graphene surface than the CNT surface by ∼0.15 eV/nm. This energy difference arises due to the relatively stronger interaction of Nylon 6 with the flat graphene surface than with the curved CNT surface. A relatively small energy difference between these two configurations clearly suggests that both the complexes may be observed in experimental studies. We further noticed that the presence of SW defects in carbon nanomaterials has practically no effect on the computed interaction energies between Nylon 6 and CNT + graphene complexes. However, it should be noted that present result is obtained by considering only the monomer of the Nylon 6 which does not mimic the approximate surface of the polymer involved in such interactions. It would involve consideration of several monomers of Nylon 6 to mimic the polymer surface and predict the influence of SW defects in relative surface interactions. However, consideration of such a larger polymeric system is beyond the scope of the current work and would be detailed somewhere else. When comparing these results with that of Nylon 6-carbon nanomaterial interactions presented in Sec. III B (Table V), we find that Nylon 6 interacts only with either CNT or graphene, of the CNT + graphene complex, whichever is located closer to it. Because of the distance dependency of the vdW interactions, the atoms of Nylon 6 (a single chain with only 19 atoms) only interact (approximately) with the atoms of CNT (or graphene) within a given distance. The interaction of Nylon 6 with the farther carbon nanomaterial is negligibly small, which does not contribute much on the computed interaction energy between Nylon 6 and the CNT + graphene complex.

The nature of interaction between Nylon 6 and the CNT + graphene complex is further confirmed by electronic charge density difference maps shown in Fig. 11. As stated earlier,

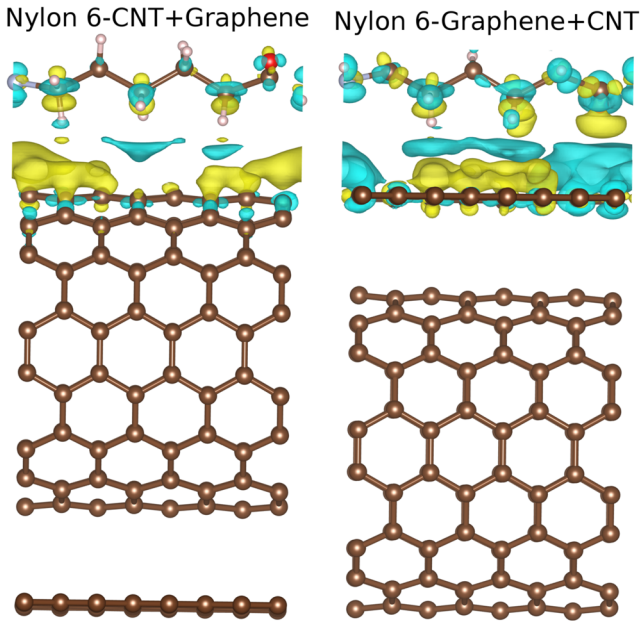

FIG. 11. Isosurfaces depicting electronic charge density difference for the interactions of Nylon 6 with CNT + graphene complex as obtained from the vdW-DF2 functional. Yellow and cyan regions represent isosurfaces for gain and loss of charge densities, respectively. The isosurface corresponds to 1.7×10^{-4} |*e*|/Bohr^3.

these maps were obtained by subtracting the charge densities of individual Nylon 6 and CNT + graphene within the adsorbed complex geometry from the charge density of the adsorbed complex, all calculated at the same level of theory. The charge accumulation and charge depletion regions are represented by yellow and cyan colors, respectively. In Fig. 11, we clearly observe that Nylon 6 only interacts with either CNT or graphene, of the CNT + graphene complex, whichever is closer to it. This observation clearly suggested that the interfacial interaction of Nylon 6 with the CNT + graphene complex takes place via weak forces, and there is no covalent character bonding among them.

We finally calculated the Young's modulus of Nylon 6-CNT + graphene complex using the energy-strain curve shown in Fig. 12. The simulated Young's modulus of the Nylon

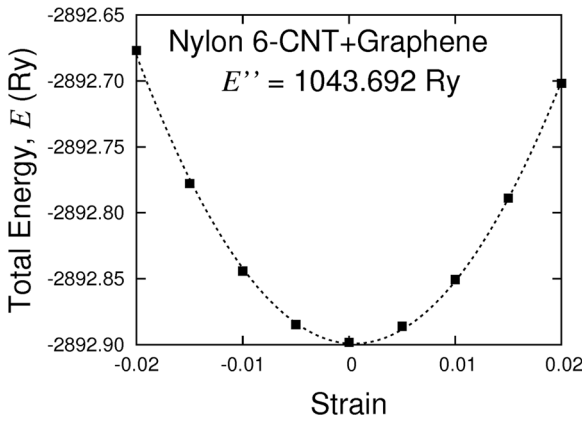

FIG. 12. Variation of total energy as a function of strain for Nylon 6-CNT + graphene complex. The dotted line represents the quadratic polynomial fit, and E'' is the curvature of energy-strain data.

6-CNT + graphene complex was 1043 GPa. Upon comparing this value with the modulus of CNT + graphene obtained in Sec. III A, Table IV (i.e., 1048 GPa), we find that the modulus of the CNT + graphene complex is slightly lowered upon the adsorption of Nylon 6. As Nylon 6 is a soft-material (polymer), we believe that the decrease in the modulus of CNT + graphene observed in our study is reasonable. The Young's modulus of the Nylon 6-CNT + graphene complex was found to be the average of the moduli of its individual constituents.

IV. CONCLUSIONS

In this paper, we have investigated the mechanism of interfacial interactions among graphene, CNTs, and Nylon 6 using first-principles DFT and empirical force-field levels of theory within properly addressed van der Waals interactions. Plane-wave DFT calculations were performed using the Quantum ESPRESSO electronic structure code, whereas the empirical calculations were performed using a class 2 force-field. Our calculations showed that the presence of SW defects on graphene does not affect the CNT-graphene interaction energies much, but the presence of defects on CNTs weakens the CNT-graphene interactions. The computed interaction energies also suggested that graphene can aid the dispersion of CNTs in Nylon 6 media. We observed that carbon nanomaterials form stable complexes with Nylon 6, and the electronic charge density difference maps revealed that the van der Waals interactions play a key stabilizing role in the interfacial interactions among graphene, CNTs, and Nylon 6. The computed electronic densities of states showed that the electronic structures of graphene and CNTs were not significantly modified, particularly around the Fermi level, due to their interactions with the Nylon 6. Our simulations indicated that the Young's moduli of graphene and CNTs were lowered by their interactions with Nylon 6. Furthermore, the presence of SW defects in carbon nanomaterials also diminished their Young's moduli. The computed interaction energies between graphene and CNTs, and carbon nanomaterials and Nylon 6 obtained from the class 2 force-field showed a good match with the DFT results and indicated the suitability of the class 2 force-field to study the properties of carbon-based materials. Thus, our first-principles results serve a benchmark for the class 2 force-field used in the current atomistic simulations.

SUPPLEMENTARY MATERIAL

See supplementary material for the charge density difference maps and electronic densities of states of the complexes involving compressed monomer of Nylon 6 with carbon nanomaterials.

ACKNOWLEDGMENTS

The use of trade, product, or firm names in this report is for descriptive purposes only and does not imply endorsement by the U.S. Government. The tests described and the resulting data presented herein, unless otherwise noted, are based upon work partly supported by the U.S. Army Basic

Research Program under No. PE 61102, Project T22, Task 01 "Military Engineering Basic Research". Permission was granted by the Director EL to publish this information. The findings of this report are not to be construed as an official Department of the Army position unless so designated by other authorized documents. S.K.J., M.R., G.T., and G.S. acknowledge the startup funds from The University of Southern Mississippi. The authors acknowledge HPC at The University of Southern Mississippi supported by the National Science Foundation under the Major Research Instrumentation (MRI) program via Grant No. ACI 1626217.

[1]K. S. Novoselov, A. K. Geim, S. V. Morozov, D. Jiang, Y. Zhang, S. V. Dubonos, I. V. Grigorieva, and A. A. Firsov, Science **306**, 666 (2004).
[2]C. Lee, X. Wei, J. W. Kysar, and J. Hone, Science **321**, 385 (2008).
[3]K.-t. Lau, C. Gu, and D. Hui, Composites, Part B **37**, 425 (2006).
[4]A. K. Geim and K. S. Novoselov, Nat. Mater. **6**, 183 (2007).
[5]S. Bal and S. Samal, Bull. Mater. Sci. **30**, 379 (2007).
[6]E. Bekyarova, S. Sarkar, S. Niyogi, M. Itkis, and R. Haddon, J. Phys. D: Appl. Phys. **45**, 154009 (2012).
[7]I. V. Magedov, L. V. Frolova, M. Ovezmyradov, D. Bethke, E. A. Shaner, and N. G. Kalugin, Carbon **54**, 192 (2013).
[8]H. Y. Mao, Y. H. Lu, J. D. Lin, S. Zhong, A. T. S. Wee, and W. Chen, Prog. Surf. Sci. **88**, 132 (2013).
[9]L. V. Frolova, I. V. Magedov, A. Harper, S. K. Jha, M. Ovezmyradov, G. Chandler, J. Garcia, D. Bethke, E. A. Shaner, I. Vasiliev *et al.*, Carbon **81**, 216 (2015).
[10]E. Yoo, J. Kim, E. Hosono, H.-s. Zhou, T. Kudo, and I. Honma, Nano Lett. **8**, 2277 (2008).
[11]U. Khan, I. O'Connor, Y. K. Gun'ko, and J. N. Coleman, Carbon **48**, 2825 (2010).
[12]Q. Su, Y. Liang, X. Feng, and K. Müllen, Chem. Commun. **46**, 8279 (2010).
[13]X. Dong, B. Li, A. Wei, X. Cao, M. B. Chan-Park, H. Zhang, L.-J. Li, W. Huang, and P. Chen, Carbon **49**, 2944 (2011).
[14]D. Cai, M. Song, and C. Xu, Adv. Mater. **20**, 1706 (2008).
[15]X. Wang, J. Yang, R. Li, H. Jiang, and Y. Li, J. Comput. Chem. **36**, 717 (2015).
[16]S. Grimme, J. Comput. Chem. **27**, 1787 (2006).
[17]A. J. Stone and D. J. Wales, Chem. Phys. Lett. **128**, 501 (1986).
[18]L. Li, S. Reich, and J. Robertson, Phys. Rev. B **72**, 184109 (2005).
[19]J. Ma, D. Alfè, A. Michaelides, and E. Wang, Phys. Rev. B **80**, 033407 (2009).
[20]L. Jiang, X.-P. Shen, J.-L. Wu, and K.-C. Shen, J. Appl. Polym. Sci. **118**, 275 (2010).
[21]B. Arash, Q. Wang, and V. Varadan, Sci. Rep. **4**, 64791 (2014).
[22]D. Qian, E. C. Dickey, R. Andrews, and T. Rantell, Appl. Phys. Lett. **76**, 2868 (2000).
[23]T. Ramanathan, A. Abdala, S. Stankovich, D. Dikin, M. Herrera-Alonso, R. Piner, D. Adamson, H. Schniepp, X. Chen, R. Ruoff *et al.*, Nat. Nanotechnol. **3**, 327 (2008).
[24]T. Zhou, X. Wang, X. Liu, and D. Xiong, Carbon **48**, 1171 (2010).
[25]T. Ramanathan, S. Stankovich, D. Dikin, H. Liu, H. Shen, S. Nguyen, and L. Brinson, J. Polym. Sci., Part B: Polym. Phys. **45**, 2097 (2007).
[26]R. Atif and F. Inam, Beilstein J. Nanotechnol. **7**, 1174 (2016).
[27]L. S. Loo and K. K. Gleason, Macromolecules **36**, 2587 (2003).
[28]C. Quarti, A. Milani, B. Civalleri, R. Orlando, and C. Castiglioni, J. Phys. Chem. B **116**, 8299 (2012).
[29]W. D. Zhang, L. Shen, I. Y. Phang, and T. Liu, Macromolecules **37**, 256 (2004).
[30]J. Gao, M. E. Itkis, A. Yu, E. Bekyarova, B. Zhao, and R. C. Haddon, J. Am. Chem. Soc. **127**, 3847 (2005).
[31]H. Mahfuz, A. Adnan, V. K. Rangari, M. M. Hasan, S. Jeelani, W. J. Wright, and S. J. DeTeresa, Appl. Phys. Lett. **88**, 083119 (2006).
[32]Z. Xu and C. Gao, Macromolecules **43**, 6716 (2010).
[33]S. Das, A. S. Wajid, J. L. Shelburne, Y.-C. Liao, and M. J. Green, Appl. Mater. Interfaces **3**, 1844 (2011).
[34]A. O'Neill, D. Bakirtzis, and D. Dixon, Eur. Polym. J. **59**, 353 (2014).
[35]P. Giannozzi, S. Baroni, N. Bonini, M. Calandra, R. Car, C. Cavazzoni, D. Ceresoli, G. L. Chiarotti, M. Cococcioni, I. Dabo *et al.*, J. Phys.: Condens. Matter **21**, 395502 (2009).
[36]M. Dion, H. Rydberg, E. Schröder, D. C. Langreth, and B. I. Lundqvist, Phys. Rev. Lett. **92**, 246401 (2004).
[37]K. Lee, E. D. Murray, L. Kong, B. I. Lundqvist, and D. C. Langreth, Phys. Rev. B **82**, 081101 (2010).
[38]A. M. Rappe, K. M. Rabe, E. Kaxiras, and J. Joannopoulos, Phys. Rev. B **41**, 1227 (1990).
[39]See http://www.quantum-espresso.org for pseudopotentials H.pbe-rrkjus.UPF, C.pbe-rrkjus.UPF, N.pbe-rrkjus.UPF, and O.pbe-rrkjus.UPF.
[40]J. Wong, S. Yadav, J. Tam, and C. V. Singh, J. Appl. Phys. **115**, 224301 (2014).
[41]S. Yadav, Z. Zhu, and C. V. Singh, Int. J. Hydrogen Energy **39**, 4981 (2014).
[42]M. K. Shukla, J. Wang, and J. Seiter, J. Phys. Chem. C **121**, 11560 (2017).
[43]S. K. Jha, M. Roth, G. Todde, J. P. Buchanan, R. D. Moser, M. K. Shukla, and G. Subramanian, J. Phys. Chem. C **122**, 1288 (2018).
[44]R. Shahsavari, M. J. Buehler, R. J.-M. Pellenq, and F.-J. Ulm, J. Am. Ceram. Soc. **92**, 2323 (2009).
[45]H. Sun, J. Phys. Chem. B **102**, 7338 (1998).
[46]S. J. Plimpton, J. Comput. Phys. **117**, 1 (1995).
[47]W. A. Saidi, J. Phys. Chem. C **117**, 9864 (2013).
[48]Y. J. Dappe, J. Ortega, and F. Flores, Phys. Rev. B **79**, 165409 (2009).
[49]B. M. Nardelli, B. I. Yakobson, and J. Bernholc, Phys. Rev. B **57**, R4277 (1998).
[50]D. R. Holmes, C. W. Bunn, and D. J. Smith, J. Polym. Sci. **17**, 159 (1955).
[51]F. Tournus, S. Latil, M. Heggie, and J.-C. Charlier, Phys. Rev. B **72**, 075431 (2005).
[52]A. AlZahrani, Appl. Surf. Sci. **257**, 807 (2010).
[53]K. Momma and F. Izumi, J. Appl. Crystallogr. **44**, 1272 (2011).
[54]F. Memarian, A. Fereidoon, and M. D. Ganji, Superlattices Microstruct. **85**, 348 (2015).
[55]K. Z. Milowska and J. A. Majewski, Phys. Chem. Chem. Phys. **15**, 14303 (2013).
[56]C. Rajesh, C. Majumder, H. Mizuseki, and Y. Kawazoe, J. Chem. Phys. **130**, 124911 (2009).
[57]M. Hammouri, S. K. Jha, and I. Vasiliev, J. Phys. Chem. C **119**, 18719 (2015).
[58]Y. Baskin and L. Meyer, Phys. Rev. **100**, 544 (1955).
[59]O. Leenaerts, B. Partoens, and F. Peeters, Phys. Rev. B **77**, 125416 (2008).
[60]S. Laref, A. Asaduzzaman, W. Beck, P. Deymier, K. Runge, L. Adamowicz, and K. Muralidharan, Chem. Phys. Lett. **582**, 115 (2013).
[61]M. Hassan, M. Walter, and M. Moseler, Phys. Chem. Chem. Phys. **16**, 33 (2014).
[62]J. Kleis, E. Schröder, and P. Hyldgaard, Phys. Rev. B **77**, 205422 (2008).
[63]M. K. Shukla and F. Hill, J. Phys. Chem. C **117**, 13136 (2013).
[64]J. Rohrer and P. Hyldgaard, Phys. Rev. B **83**, 165423 (2011).
[65]L. Van Hove, Phys. Rev. **89**, 1189 (1953).
[66]F. Hao, D. Fang, and Z. Xu, Appl. Phys. Lett. **99**, 041901 (2011).
[67]J. Jilili, A. Abdurahman, O. Gülseren, and U. Schwingenschlögl, Appl. Phys. Lett. **105**, 013103 (2014).